SYNTHESIS OF RUTILE-TiO$_2$ NANOROD ARRAYS FOR EFFICIENT SOLAR WATER SPLITTING VIA MICROWAVE-ASSISTED HYDROTHERMAL METHOD

A. K.QASIM [a*], L. A. JAMIL[b], A. F. ABDULRAHMAN [c]

[a]*Dept. of Environment, Faculty of Science, University of Zakho, Zakho, Kurdistan Region, Iraq*
[b]*Dept. of Chemistry, Faculty of Science, University of Zakho, Zakho, Kurdistan Region, Iraq*
[c]*Dept. of Physics, Faculty of Science, University of Zakho, Zakho, Kurdistan Region, Iraq*

Using a microwave-assisted hydro thermal method (MWAHM) a single crystalline of vertically aligned TiO$_2$ nanorod (NR) arrays has been achieved via the novel ultra-rapid synthetic method for the production. High-quality NR arrays with controlled film thickness were achieved with fine control of the growth conditions as well. The effect of the different reaction conditions of MWAHM such as reaction time and growth temperature on the morphology, crystal orientation, and photo catalytic activity have been systematically investigated. In a typical condition of the MWAHM using 0.4 cm^3 of titanium(IV) n-butoxide (TBO) at 180 °C for 40 minutes, a small diameter of 124 nm and short length 2.93 μm of TiO$_2$ nanorods, are grown on fluorine-doped tin oxide (FTO) substrate. However, the photo current density produced TiO$_2$ NRs of 2.90 mA cm^{-2} with a maximum photo conversion efficiency of about 2.7% which confers excellent photo-electrochemical performance. In comparison with the typical hydro thermal method (HM) synthesized NRs, the ultra-fast MWAHM synthesized NRs offers five times more efficiency photoelectrochemical (PEC) water splitting than the hydro thermal method (HM). The results suggest that these dense and aligned one-dimensional TiO$_2$ nanorods are promising for hydrogen generation from water splitting based on PEC cells.

1. Introduction

Photoelectrochemical (PEC) water splitting has been researched extensively for efficient harvesting of solar energy in H$_2$ gas [1, 2]. A number of nanostructured metal oxide semiconductors, such as titanium dioxide TiO$_2$ and zinc oxide (ZnO), are suitable for this application, due to their wide band gap [3] and good electrical properties with high catalytic activity and excellent stability in many solvents over a wide pH range [4-6].

Much literature has been published employing a number of different strategies to enhance the photoconversion efficiency through doping [7-9], sensitizing [10,11], and plasmonic enhancement [12, 13]. For example, Cu, Br, and Y-doped TiO$_2$ nanorods have shown significant enhancement in either UV or visible light sensitivity [14-16]. One of the most promising TiO$_2$ structures, vertically aligned nanorod arrays (NRs), have demonstrated a great potential to achieve high diffusion coefficient of carriers in electric devices due to their unique one-dimensional (1D) structure, high surface area and charge transport property [17]. Metal oxide nanowires are highly effective materials for solar water splitting, However, titanium dioxide (TiO$_2$) nanostructured materials have attracted considerable attention because of their applications in various fields such as in dye-sensitized solar cells [18], photocatalysis [19, 20], photoelectrochemical applications [21], and water splitting [22, 23] .

---

* Corresponding authors: amin.qasim@uoz.edu.krd

In this study the microwave-assisted hydrothermal method (MWAHM) for deposition of vertically aligned of rutile-TiO$_2$ nanorod arrays applied as a photoanode for the photolysis of water. Due to offers more rapid heating, faster kinetics, higher yield, better reproducibility of products and heating the sample internally compared with conventional heating. In microwave heating, unlike conventional heating, heat is created within the material itself rather than heating provided from external sources. Subsequently, not only were NRs grown in a fraction of the time compared to conventional methods, the synthesis led to a high density of surface defects with increased n-type doping. This heating mechanism also results in the reduction of the reaction time, the microwave (MW) NRs showed a great increase in photoconversion efficiency for water splitting compared to the chemical bath deposition (CBD) and hydrothermal method (HM) sample.

Microwave assisted synthetic methods have been applied to a number of TiO$_2$ nanostructures [24-28]. Vertically aligned TiO$_2$ NR arrays have appeared recently in the literature with limited control of morphology. They are used as a photocatalyst [29] and in a gas ionization sensor [30]. In both cases, enhanced electronic properties were observed and this was attributed to increased oxygen vacancies from rapid crystallization. In this work, a novel MWAHM for the growth of TiO$_2$ NR arrays is presented and their solar water splitting ability is compared to a conventional hydrothermal method. The NR arrays show a high density of defects, which is responsible for the increase in PCE conversion efficiency over the conventional hydrothermal NRs by a factor of 5. The populations of these defects were then controlled using thermal annealing in air at various temperatures to double the efficiency achieved. This yielded a photocurrent density of 0.893 mA cm^{-2} at 1 V potential bias vs KCl saturated Ag/AgCl reference electrode.

2. Experimental method

A. Synthesis of TiO$_2$ Nanorods

All chemicals used were purchased from Sigma-Aldrich with no further purification Hydrochloric acid (32 wt. %, d= 1.16), titanium (IV) n- butoxide (99+ %) and. Transparent conductive fluorine-doped tin oxide (FTO) with diameter (D= 2mm, 7Ω/sq.) sheet glass was used as the substrate, cut into sample sizes of 1×2 cm^2. The substrate was cleaned by sonication successively in methanol, isopropanol, and then deionized (DI) water, for 20 min each, followed by drying in air.

In the MWAHM method, the FTO glass (1 x 2 cm^2) substrate was placed in a 35 mL microwave vessel with 12 mL of growth solution, hydrochloric acid (14 ml of 32% HCl by Wt. %) was added to DI water (10 ml) and magnetically stirred for 5 minutes, after which, titanium butoxide (TBO, 0.4 ml) was added to the reaction solution and magnetically stirred for a further 5 minutes. The microwave (Discover SP, CEM) was set to different temperatures (170, 180, 190, 200 °C) for (20, 30, 40 and 50 min) at a power of 100 W; no stirring was used to avoid disturbing the crystal growth, all samples were rinsed with DI water. Annealing in the air was performed using a tube furnace for 3 h at 550 °C to optimize the crystal defect concentration and adhesion of NRs to the substrate subsequently as shown in the Fig (1). For comparison, a previously developed hydrothermal method was also used [31]. To achieve a similar length of NRs in hydrothermal method, the FTO glass (1 x 2 cm^2) substrate was placed in autoclave with 24 ml of the growth solution at 160 °C for 4 h, The autoclave was sealed and placed in the gas chromatography (GC) oven.

B. Structural and physical characterization

The cross section and surface morphologies were observed using scanning electron microscopy (SEM, JSM820M, Jeol). The crystallinity and structural orientation of the nanostructures were analyzed by powder X-ray diffractometer (XRD, Siemens D500), all the samples were measured in the continuous scan mode in the 2θ range of 20-70°, using a scan rate of 0.02 deg/s. The nanorod length and diameters were measured by SEM images using Image J software (National Institutes of Health, USA).

C. Water Splitting and Optoelectronic Measurement

PEC water splitting performances were measured using a standard three electrode setup. A KCl saturated Ag/AgCl electrode was used as the reference and platinum foil was used as the counter electrode. TiO$_2$ NR arrays grown on FTO-glass substrate were used as the photoanode. A potentiostat (EA163, eDAQ) was used to control the voltage bias and to measure the photocurrent. The voltage was scanned from − 0.6 to 1.2 V, and the electrolyte used in the PEC cell was 1M KOH (with measured pH of 13.2). No additional scavenging chemicals were added to the electrolyte. In order to simulate sunlight, a 300 W xenon lamp with AM 1.5 filters was used as the light source. The power intensity of the light was adjusted to 100 mW/cm^2. Finally the photo absorption spectra used to calculate the band gap with Tauc plots were examined using a UV−Vis spectrophotometer (Thermospectronic UV 300).

3. Optical properties

To determine the optical properties of the TiO$_2$ NR films, the integrating sphere (Ocean Optics ISP-REF), is used to measure the reflectance of the thick nanorods (NRs) film and allow photon transmission to happen. The UV-Vis absorption was used to measure the band gaps of the TiO$_2$ nanostructures. In this study, both MW NRs and HM NRs samples were prepared on FTO glass substrates.
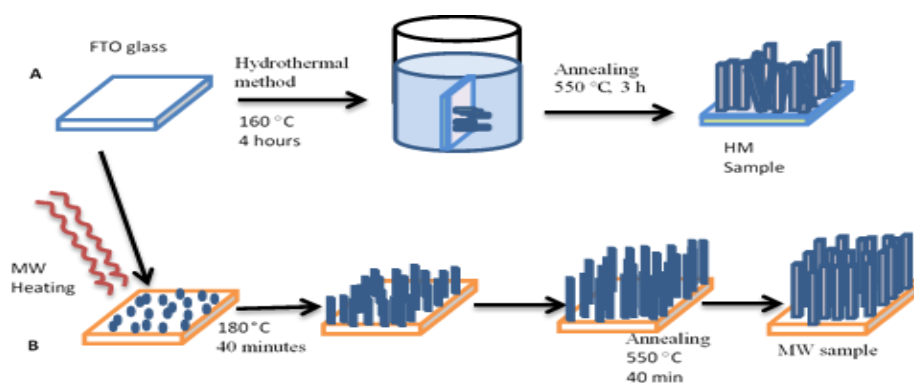

Fig. 1. Schematic diagram of proposed formation mechanism of TiO$_2$ NRs:
(a) Hydrothermal method, and (b) MWAHM.

4. Results and discussion

4.1. Morphology and crystal structure of TiO$_2$ NRs film via MWAHM
A. Effect of reaction time of MW on the TiO$_2$ nanorods

To accurately study the growth rate of the rutile nanorods, a series of the nanorods growth experiments were conducted as a function of the growth time (30, 40, and 50min). As shown in Fig. 2, the TiO$_2$ NRs is observed perpendicular to the surface and grows in a very high density over the entire FTO/glass substrates, both diameter and length of the nanorods increases with reaction time as in Fig. 3(A, B).

The diameter distribution and length of the nanorods are plotted in Fig. 3(A, B). It is noted that both diameter and length of the nanorods increase with reaction time, and the titanium nanorods (TNRs) obtained after different reaction times have a mono- dispersed diameter. The nanorods after 30 min of growth are about 1.3 μm in length and 93 nm in diameter with crystal domain size and FWHM 9.45 nm and 0.5° respectively. As the growth time is increased to 40 min, the average NRs length and diameter are increased to about 2.06 μm and 120 nm respectively, with crystal domain size and FWHM 13.45 nm and 0.8° respectively. Growing the reaction time of MW 50 min produces a large increase in rod diameter and length of NRs, 135 nm and length 2.75

μm, with crystal domain size and FWHM to be 15.02 nm and 0.73° respectively. Therefore, decreasing of FWHM and increasing of the crystal size domain, indicating the formation of nanorods with a more varied diameter at a longer growth time and the rods start to merge together and TiO$_2$ NRs delaminates from the FTO.

Fig. 2B shows the uniform rutile crystal morphology of the NRs synthesized from the MWAHM method. The average diameter of the NRs was determined to be 120 ± 22 nm comparable to the NRs synthesized using the conventional hydrothermal method. A small fraction of the rods appears irregular in shape, occurring from the coalescing of rods due to their rapid growth rate. It is noted that the growth rate of the nanorods in the MW-assisted hydrothermal reaction is much faster than in the conventional hydrothermal reaction. When the nanorods were grown at 180 °C for 40 min in the M-W reactor, the nanorods were as long as 2.06 μm. In the purely hydrothermal reaction, the growth of the nanorods with the same length needs more than 10 h. This accelerated reaction rate is traced to the unique heating mechanisms of the microwave assisted reaction, such as volumetric heating.
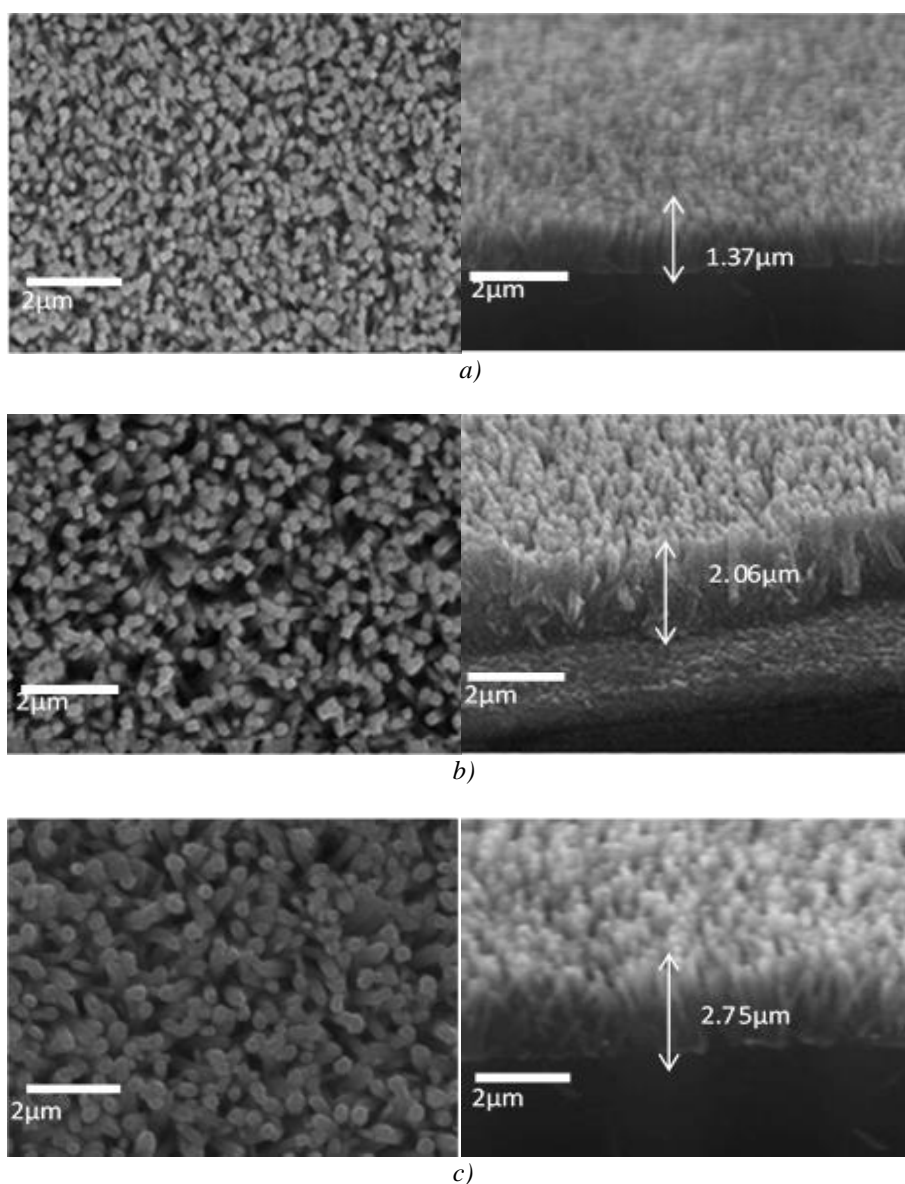

a)

b)

c)

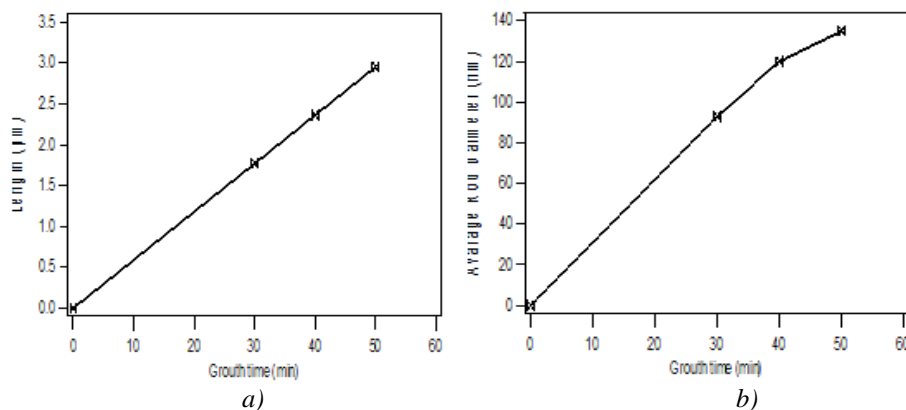*Fig. 2. SEM image of TiO$_2$ nanorods at different reaction time (a)30, (b) 40, and (c) 50 min).*

Fig. 3. (a) Length and (b) Diameter of TiO₂ nanorods arrays with different reaction time of 30, 40 and 50 min of MWAHM.

Fig. 4 shows the change in the XRD patterns as a function of the growth time. The intensity ratio of (002) peak over (101) peak represents the degree of the alignment of the rutile nanorods. The higher intensity of (101) peak indicates that the nanorods are more randomly oriented at the early stage of the growth. As the reaction time increases, the growth of the oblique nanorods is retarded and the well-aligned arrays of the vertical nanorods bury the oblique nanorods [32]. Therefore, the relative intensity of (002) increases as the growth time increases [33]. This explanation of the change in the orientation of the nanorods is supported by SEM micrographs in Fig. 2B.
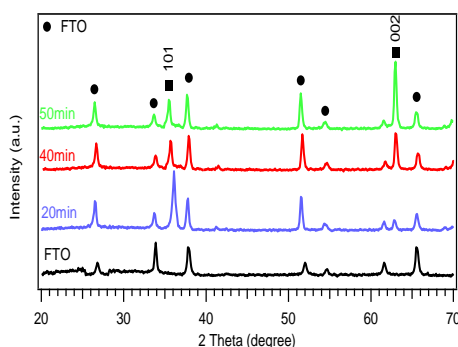

Fig. 4. XRD patterns of TiO₂ nanorod grown at 200 ᵒC for different reaction times (30, 40, and 50 min).

B. Effect of growth temperature of MW on the TiO₂ nanorods

Fig. 5 (A, B and C) show the effect of the growth temperature on the morphology of the nanorods. To compare the change in the length, and diameter of the rutile nanorods was grown at 170, 180, and 190 ᵒ C for 40 min. An increase in the reaction temperature increases both length and diameter of the nanorods. However, the growth temperature influences the length of the nanorods more than the diameter of the nanorods in the M-W-assisted hydrothermal reaction. This indicates that the nanorods grown at relatively high temperature 180ᵒ C are suitable for their application to electrochemical water splitting due to their higher surface area. Fig. 6(A and B) shows the diameter distribution (monodispersity) and the length of the TNRs formed at different growth temperatures. It confirms that the rods have monodisperse diameters. Nanorods with an average diameter of 88nm (FWHM of 16.23ᵒ) and length is 2.75 µm were formed at 170ᵒC. Increasing the MW temperature to 180ᵒC saw the average diameter rise significantly with broadening of the FWHM to more than 29 nm, which indicate the large difference in the size of the rods formed at high temperature. While the temperature of the MW is increased to 190°C the average nanorods diameter expands to 148 nm, the length is 3.35 µm and the crystal domain and

FWHM are changed to 14.56 nm and 0.55° respectively, which indicate that the large difference in the size of the rods formed at high temperature, at higher temperature the TNRs delaminated from the FTO substrate.
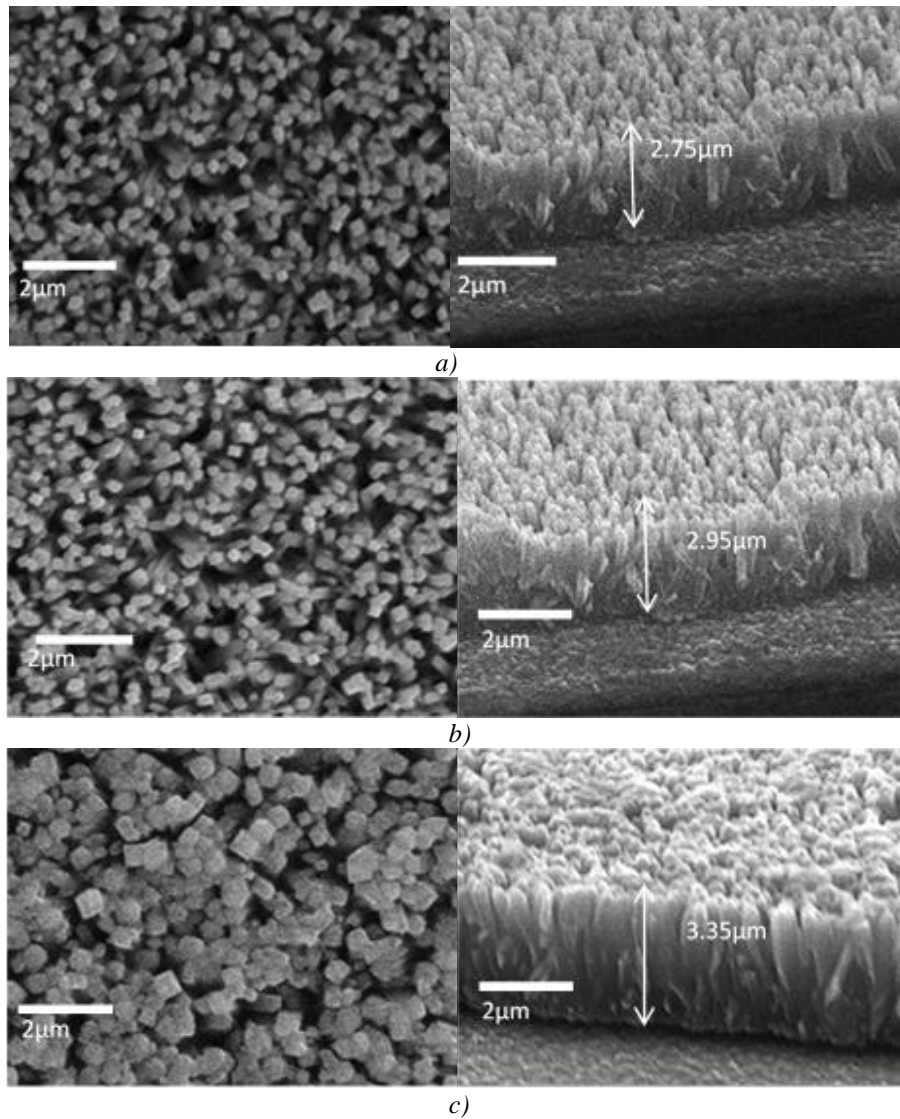

Fig. 5. SEM image of TiO$_2$ nanorods at different growth temperatures
(a) 170,(b) 180, and (c) 190 ^{o}C) for 40 min.

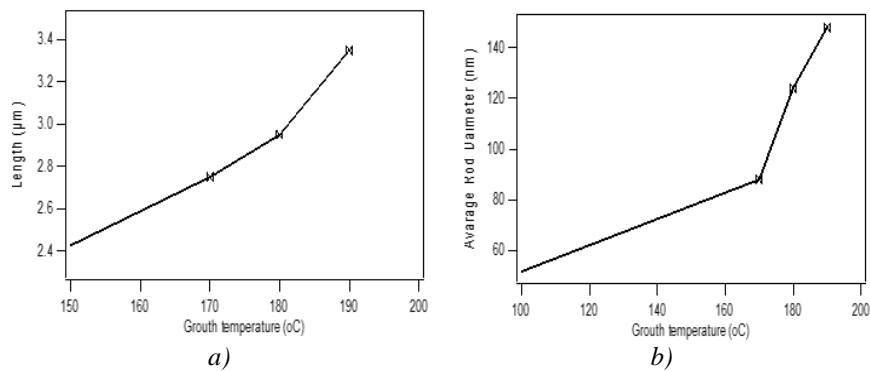*Fig. 6. (a) Length and (b) Diameter of TiO$_2$ nanorods arrays with different temperature of*
170, 180 and 190 ^{o}C of MWAHM.

Fig. 7 A reveals that the UV-Vis absorption onset of TiO_2 NRs via MW is shifted to a longer wavelength (~395 nm) as compared to NRs via HM (~372 nm). The red shift of TiO_2 NRs via MW indicates that the optical band gap of NRs sample via MW is smaller than NRs via HM. The band gap of the semiconductor film was determined from the Tauc Eq (1.1)[34-36].

$$Ah\nu = A^o(h\nu - E_g)^r \quad (1)$$

where α is the absorption coefficient, E_g is the band gap energy, h denotes the Planck's constant, hν is the photon energy $(h\nu = \frac{hc}{\lambda(nm)} = \frac{1240}{\lambda(nm)}$ eV), υ represents the frequency of the incident photon, c it is speed of light and A_o is a constant that depends on the electron-hole mobility of the material and n depends on the nature of transitions of the semiconductor. The r has the values of 1/2 and 2 for allowing direct and indirect transitions, respectively. The linear nature of the Tauc plots (Fig. 7.B) at the absorption edge confirms that the films are semiconductors with direct band gaps. The band gap energy was 2.81 eV, which is a significant red shift from the 2.94 eV for the HM sample in association with the high defect density. Such a decrease would allow the TiO_2 to absorb the leading edge of the visible spectrum which enhances its photocatalytic activity and photoelectrochemical water splitting [8].
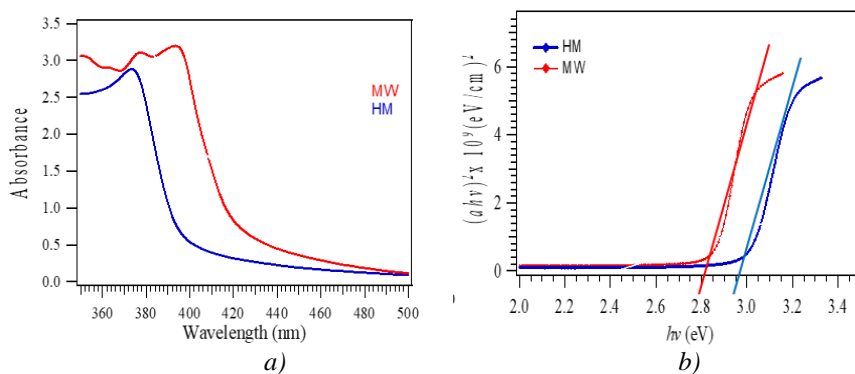

Fig. 7. (a)UV-Vis absorption spectra of TiO_2 NRs for MW at 40min and 180°C, and for HM at 4h and 160°C and (b) Tauc plots.

C. PEC Water Splitting Performance

The photocatalytic activity of the MWAHM TiO_2 NRs with a high density of defects was investigated in PEC water splitting. In comparison with low defect density HM NRs, a much higher PEC water splitting activity was observed from the MWAHM TiO_2 NRs.
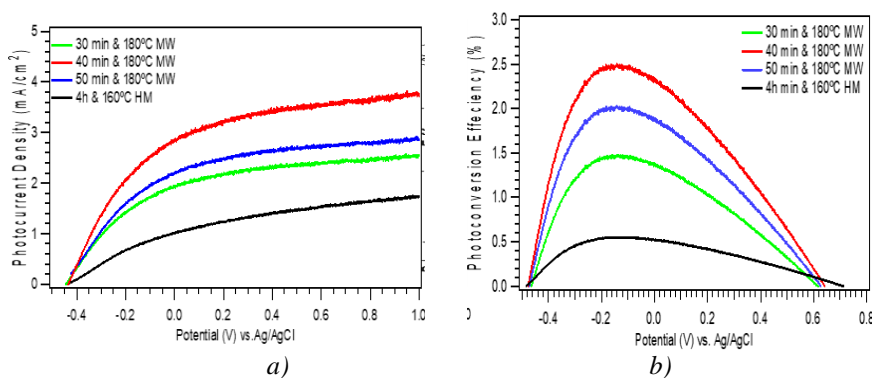

Fig. 8. I-V curve of Photocurrent generated from TiO_2 NR films with the dark and under simulated AM 1.5 irradiation in 1.0 M KOH electrolyte (pH= 13.2) under the illumination of a 100 mW cm^{-2} solar simulator which were prepared under different MW and HM conditions (a) photocurrent densities and (b) photoconversion efficiency curves.

Shown in Fig. 8(a, b) the photocurrent of 2.80 mA cm^{-2} was achieved from the MW at 40 min and 180° C samples with respect to the 0.95 mA cm^{-2} from the HM sample, although both have almost identical nanostructures. However, Fig.8 (A and B), shows the photocurrent density and the photoconversion efficiency of the PEC mad with the as prepared TiO$_2$ electrode at different growth times (30, 40 and 50 min) but temperature kept constant at 180 ℃ for MW and 160℃ for HM, At a short reaction time (30 min) the sample produced a photocurrent density of 1.9 mAcm^{-2} at 0.10 potential V vs. Ag/AgCl and showed a photo conversion efficiency of 1.7% at - 0.16V. Increasing the time to (40 min) showed the photocurrent increase to the extreme of 2.9 mAcm^{-2} at 0.20 potential V vs. Ag/AgCl. This value was corresponds to the highest photo efficiency of 2.7% at -0.16 V. Further increasing the growth time to (50 min) induces both photocurrent density and photoconversion efficiency to 2.20 mAcm^{-2} and 2.1% because the nanorod density and film thickness increase at high growth time and prevents UV light from penetrating through the nanorods film and therefore reduces the light absorption efficiency.

The corresponding photoconversion efficiencies were plotted in Fig. 8B. A similar trend can be found as the photocurrent and the best photoconversion performance was achieved from the MW sample growth time at 40 min with maximum photoconversion efficiency of 2.7%, which is 5 times higher with respect to the value from the HM NRs (0.5%).

5. Conclusions

In this study a novel ultra-rapid microwave assisted hydrothermal method for the production of TiO$_2$ NR arrays has been demonstrated. For the first time MWAHM TiO$_2$ NR arrays are applied to PEC water splitting with significantly higher efficiency. The inclusion of a high population of crystal defects has led to controlling the condition of MWAHM such as growth time and temperature and a significant enhancement in water splitting. TiO$_2$ NR arrays density was optimized from MW condition such as growth time and temperature to 40 min and 180 ℃ respectively. This led to a 5-fold increase in photoconversion efficiency from the HM sample. Further increasing the growth time and temperature more than 40 min and 180 ℃ respectively, led to decrease the photoconversion efficiency, which behaves as a hole trap and shifts the flat-band potential toward the valence band. This in turn led to a reduction in the PEC performance.

References

[1] A. Fujishima, K. Honda, Nature **238**(5358), 37 (1972).
[2] M. G. Walter et al., Chemical reviews **110**(11), 6446 (2010).
[3] Ahmed Fattah, Sabah Mohammed Ahmed, and Naser Mahmoud Ahmed, Science Journal of University of Zakho **6**(4): p. 160 (2018).
[4] D. Chen et al., Industrial & Engineering Chemistry Research **45**(12), 4110 (2006).
[5] P. Mishra, P. Shukla, O. Srivastava, International Journal of Hydrogen Energy **32**(12), 1680 (2007).
[6] A. F. ABDULRAHMAN, S. M. AHMED, N. M. AHMED, and M. A. ALMESSIERE, Digest Journal of Nanomaterials and Biostructures, **11**(4): p. 1073 (2016).
[7] L. Cai et al., International Journal of Hydrogen Energy **40**(3), 1394 (2015).
[8] W. C. Lee et al., International Journal of Hydrogen Energy **41**(1), 123 (2016).
[9] H. J. Lee et al., Journal of Materials Chemistry A **4**(9), 3223 (2016).
[10] S. Mukhopadhyay et al., Physical Chemistry Chemical Physics **17**(31), 20407 (2015).
[11] N. M. Vuong et al., The Journal of Physical Chemistry C **119**(43), 24323 (2015).
[12] J. Lu et al., Journal of Alloys and Compounds **617**, 869 (2014).
[13] M. Wu et al., ACS applied materials & interfaces **6**(17), 15052 (2014).
[14] C. Zhang et al., Nano Energy **12**, 231 (2015).
[15] M. Wang et al., Scientific reports **5**, 12925 (2015).

[16] Qasim, A.K., L.A. Jamil, and Q. Chen, Science Journal of University of Zakho, **5**(1): p. 79 (2017).

[17] Law, M., et al., Nanowire dye-sensitized solar cells. Nature materials, 2005. 4(6): p. 455.

[18] M. Law et al., Journal of the American Chemical Society **130**(40), 13364 (2008).

[19] S. P. Albu et al., Nano letters **7**(5), 1286 (2007).

[20] K. Hashimoto, H. Irie, A. Fujishima, Japanese journal of applied physics **44**(12R), 8269 (2005).

[21] H. Zhang et al., Langmuir **26**(13), 11226 (2010).

[22] E. Y. Kim, J. H. Park, G. Y. Han, Journal of power sources **184**(1), 284 (2008).

[23] Qasim, A.K. and L.A. Jamil., IOP Conference Series: Materials Science and Engineering. 2018.

[24] W,-W. Wang, Y.-J. Zhu, Inorganic Chemistry Communications **7**(9), 1003 (2004).

[25] J. Huang et al., Materials Science and Engineering: B **150**(3), 187 (2008).

[26] M.-G. Ma et al., Materials Letters **62**(3), 507 (2008).

[27] N. U. Sangari, S. C. Devi, Journal of Solid State Chemistry **197**, 483 (2013).

[28] Yasin, S.A. and A.K. Qasim, Science Journal of University of Zakho, **6**(3): p. 104 (2018)

[29] S. Baruah et al., Beilstein journal of nanotechnology **1**(1), 14 (2010).

[30] T. S. Tee et al., Sensors and Actuators B: Chemical **227**, 304 (2016).

[31] Qasim, A.K., Synthesis and Applications of Metal Oxide Nanostructure Films and Construction of Copper (II) Ion-Selective Sensor based on Dithio in a PVC matrix Thesis, 2017: p. 110.

[32] A. F. ABDULRAHMAN, S. M. AHMED, and M. A. ALMESSIERE, Digest Journal of Nanomaterials and Biostructures, **12**(4): p.1001 (2017).

[33] Ahmed Fattah Abdulrahman, Sabah Mohammed Ahmed, and Naser Mahmoud Ahmed, Science Journal of University of Zakho **5**(1): p. 128 (2017).

[34] A. A. Tahir et al., Chemistry of Materials **22**(17), 5084 (2010).

[35] L. Miao et al., Applied Surface Science **212**, 255 (2003).

[36] A. F. ABDULRAHMAN, S. M. AHMED, N. M. AHMED, and M. A. ALMESSIERE, Digest Journal of Nanomaterials and Biostructures, **11**(3): p. 1007 (2016).